The Effect of Satellite Rainfall Error Modeling on Soil Moisture Prediction Uncertainty

VIVIANA MAGGIONI

Department of Civil and Environmental Engineering, University of Connecticut, Storrs, Connecticut

ROLF H. REICHLE

Global Modeling and Assimilation Office, NASA Goddard Space Flight Center, Greenbelt, Maryland

EMMANOUIL N. ANAGNOSTOU

Department of Civil and Environmental Engineering, University of Connecticut, Storrs, Connecticut

(Manuscript received 23 August 2010, in final form 23 December 2010)

ABSTRACT

This study assesses the impact of satellite rainfall error structure on soil moisture simulations with the NASA Catchment land surface model. Specifically, the study contrasts a complex satellite rainfall error model (SREM2D) with the standard rainfall error model used to generate ensembles of rainfall fields as part of the Land Data Assimilation System (LDAS) developed at the NASA Global Modeling and Assimilation Office. The study is conducted in the Oklahoma region, which offers good coverage by weather radars and in situ meteorological and soil moisture measurement stations. The authors used high-resolution (25 km, 3-hourly) satellite rainfall fields derived from the NOAA/Climate Prediction Center morphing (CMORPH) global satellite product and rain gauge–calibrated radar rainfall fields (considered as the reference rainfall). The LDAS simulations are evaluated in terms of rainfall and soil moisture error. Comparisons of rainfall ensembles generated by SREM2D and LDAS against reference rainfall show that both rainfall error models preserve the satellite rainfall error characteristics across a range of spatial scales. The error structure in SREM2D is shown to generate rainfall replicates with higher variability that better envelop the reference rainfall than those generated by the LDAS error model. Likewise, the SREM2D-generated soil moisture ensemble shows slightly higher spread than the LDAS-generated ensemble and thus better encapsulates the reference soil moisture. Soil moisture errors, however, are less sensitive than precipitation errors to the complexity of the precipitation error modeling approach because soil moisture dynamics are dissipative and nonlinear.

1. Introduction

Surface and root zone soil moisture control the partitioning of available energy incident on the land surface. For this reason, soil moisture is a key variable in the water cycle that impacts local weather, such as cloud coverage and precipitation, and hydrological parameters, such as runoff and evapotranspiration (Betts and Ball 1998). Therefore an accurate characterization of soil water content can lead to improvements not only in weather and climate prediction, but also in hazard mitigation (floods and droughts), agricultural planning, and water resources management. Arguably, soil moisture is an important parameter for the derivation of flood warning schemes based on rainfall thresholds (Martina et al. 2005; Carpenter et al. 1999). In such systems, quantitative soil moisture information is needed for the selection of the proper rainfall–runoff threshold curve to use with the estimated rainfall volume data for issuing flood warnings.

Information on soil moisture may be obtained from three main sources: ground measurements, remote sensing, and land surface models. A common approach to estimate soil moisture at regional–global scales is to run a land surface model forced with meteorological observations. The physical formulation of a land surface model integrates the atmospheric forcing and produces

Corresponding author address: Viviana Maggioni, Civil and Environmental Engineering, University of Connecticut, Storrs, CT 06269.
E-mail: viviana@engr.uconn.edu

DOI: 10.1175/2011JHM1355.1

© 2011 American Meteorological Society

estimates of soil moisture. Different sources of error affect land surface model predictions: errors in the atmospheric forcing, faulty estimates of the model parameters, and deficient model formulations (Reichle et al. 2004).

Indirect measurements of surface soil moisture can be obtained from satellite sensors that measure the microwave (MW) emission by the land surface (e.g., Jackson 1993; Njoku et al. 2003). However, satellite data coverage is spatially and temporally incomplete and retrievals are prone to errors because of limitations in the instrument sampling, difficulties in the parameterization of the physical processes that relate brightness temperature with the near-surface soil moisture, and difficulties in obtaining a global distribution of the parameters of the retrieval algorithm. Moreover, it is difficult to retrieve soil moisture in areas where the fraction of water is significant (i.e., coastal areas) and/or when the soil is frozen or densely vegetated.

Data assimilation systems merge satellite retrieval information with the spatially and temporally complete information predicted by the land surface models to provide a superior product. This is achieved by correcting the model predictions (e.g., of soil moisture) with a stochastic filtering technique that uses differences between the model predictions and satellite estimates along with the associated uncertainty of each data source. Constraining the model with observations using data assimilation methods has been demonstrated as an effective way to integrate data with models. Studies have confirmed that assimilating satellite-retrieved soil moisture improves the dynamic representation of soil moisture (Reichle et al. 2007).

The quality of the assimilation estimates depends critically on the realism of the error estimates for the model and the observations (Reichle et al. 2008). Arguably, the way model errors are handled in standard land data assimilation systems could use improvement, which should lead to better estimates. One such system is the Land Data Assimilation System (LDAS) developed at the National Aeronautics and Space Administration (NASA) Global Modeling and Assimilation Office. Specifically, LDAS applies perturbations to the model forcing and state variables to obtain an ensemble of land surface fields that reflects modeling uncertainty. Perturbations to the precipitation forcing are of particular importance to the modeling of soil moisture uncertainty, which motivates our investigation of the impact of the rainfall error model on the simulation of the soil moisture error characteristics. Specifically, the precipitation perturbations generated by the LDAS error model are spatially and temporally correlated and lognormally distributed multiplication factors. Recent studies have proposed more complex satellite rainfall error models for generating error ensembles of satellite rainfall fields (Bellerby and Sun 2005; Hossain and Anagnostou 2006a). Hossain and Anagnostou (2006a) investigated one of those rainfall error models, the multidimensional Satellite Rainfall Error Model (SREM2D), to describe the uncertainty in soil moisture predictions from a land surface model forced with satellite rainfall fields.

In this paper we seek to expand the Hossain and Anagnostou (2006a) study by conducting numerical investigations to (i) assess the impact of satellite rainfall error structure on soil moisture uncertainty simulated by the NASA Catchment land surface model (CLSM or Catchment model); (ii) contrast the more complex SREM2D rainfall error model to the standard rainfall error model used in LDAS to generate rainfall ensembles; and (iii) further investigate the propagation of precipitation errors into soil moisture errors.

We begin with a description of the experiment domain, period, and data employed in the study (section 2), followed by a brief overview of LDAS (section 3) and a description of the rainfall error schemes (section 4). In section 5, we describe the experiments and in section 6 we present and discuss our results. We conclude with the major findings in section 7.

2. Study region and data

a. Study area and period

The region of Oklahoma (OK) in the midwestern United States was chosen as the study area for its smooth terrain, good coverage by weather radars, and dense network of hydrometeorological stations from the Oklahoma Mesonet (Brock et al. 1995, their Fig. 1). The region is characterized by a continental climate associated with cold winters and hot summers. Its topography rises gently from an altitude of 88 m MSL in the southeastern corner to a height of 1515 m MSLat the tip of the ''Panhandle'' in the northwestern corner. The study region is discretized into a 25 km $\times$ 25 km Cartesian modeling grid (34°–37°N, 100°–95°W), representing a total area of about 137 500 km^2, over which radar and satellite rainfall data were interpolated (see discussion below). The western half of the domain is characterized by drier conditions, compared to the wetter eastern half, as shown by the cumulative rain map. The study period includes three continuous years from 1 January 2004 to 31 December 2006.

b. Data description

Data from various sources were used for this study. We focus on two high-resolution rainfall products: the Weather Surveillance Radar-1988 Doppler (WSR-88D)

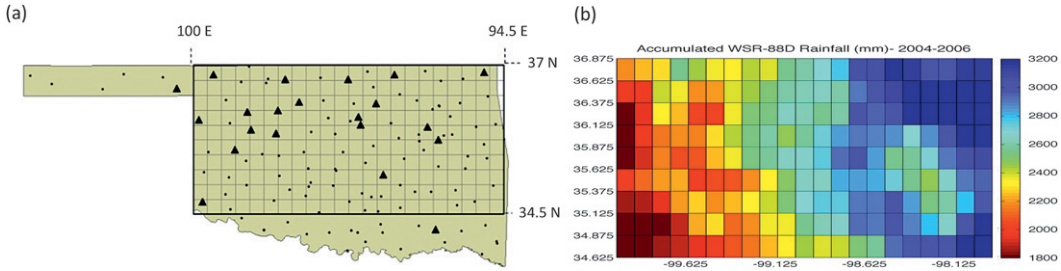

FIG. 1. (a) The 25-km grid covering the experiment domain and locations of OK Mesonet stations (black dots). The triangular symbols represent OK Mesonet stations where sufficient soil moisture observations were available at four different depths during the study period. (b) The 3-yr (2004–06) cumulative WSR-88D rainfall (mm).

radar rainfall and the National Oceanic and Atmospheric Administration (NOAA)/Climate Prediction Center morphing (CMORPH) satellite rainfall. Along with supplemental surface meteorological forcing data from the Global Land Data Assimilation System (GLDAS) project, the radar and satellite precipitation products are used to force the land surface model and generate soil moisture fields. The coarser (and global) GLDAS forcing data were chosen over the finer-scale North American LDAS (NLDAS) forcing data, as the target of this study is to include better precipitation error characterization in global land data assimilation. Finally, we also employ ground observations of soil moisture from in situ stations for a comparison with the land surface model integrations.

The radar dataset is extracted from the Stage IV National Weather Service (NWS) WSR-88D precipitation estimates with real-time adjustments based on mean-field radar–rain gauge hourly accumulation comparisons (Fulton 1998). The Stage IV product is a national mosaic of precipitation estimates based on the Stage II products from all WSR-88D radars across the continental United States. WSR-88D Stage IV data are available at 4-km resolution and hourly time steps. There are many sources of uncertainty in the WSR-88D rain-rate estimates, including the drop size distribution, the vertical structure of raindrops between the sampling volume and the ground, geometric effects of the spreading radar beam, small-scale variability of precipitation within a sampling volume, and erroneous radar echoes, such as anomalous propagation of the radar beam (Krajewski et al. 2006). The above-mentioned mean-field bias adjustment of radar rainfall toward rain gauge measurements is designed to reduce the uncertainty in radar rainfall estimates.

The satellite product used here is the NOAA/Climate Prediction Center morphing product (Joyce et al. 2004). The product interpolates successive passive microwave rainfall estimates based on high-frequency infrared (IR) images. Specifically, the algorithm uses motion vectors derived from half-hourly geostationary satellite IR imagery to interpolate the less frequent but relatively high-quality rainfall estimates obtained from low-earth orbit MW sensors. The dynamic morphological characteristics (such as shape and intensity) of precipitation features are interpolated between consecutive microwave sensor samples through time-weighted linear interpolation. This process yields spatially and temporally continuous MW rainfall fields that have been guided by IR imagery and yet are independent of IR rain retrievals. The CMORPH product is available half-hourly at 8-km resolution. It has been shown to have a high probability of rain detection as well as high temporal and spatial correlation when compared to ground-observed rainfall data across the Oklahoma region (Anagnostou et al. 2010). For this study, we regridded and aggregated the satellite and radar precipitation datasets to the 25-km modeling grid and a 3-hourly time step for analysis and input to the land surface modeling system.

The remainder of the surface meteorological forcing data (including air temperature and humidity, radiation, and wind speed) are from the GLDAS project (Rodell et al. 2004; http://ldas.gsfc.nasa.gov) based on output from the global atmospheric data assimilation system at the NASA Global Modeling and Assimilation Office (GMAO; Bloom et al. 2005). The GLDAS data used here are identical to those customized for the GMAO seasonal forecasting system (3-hourly time steps and $2° \times 2.5°$ resolution in latitude and longitude).

Besides the above-mentioned surface meteorological observations, the OK Mesonet also provides soil moisture observations that we use in our study to demonstrate the viability of the land surface modeling system. Measurements are taken at four depths (5, 25, 60, and 75 cm) and 30-min resolution at 106 automated observing stations located throughout the state (Fig. 1). The soil moisture dataset is quality controlled and includes quality flags in the dataset. For our study period, soil moisture observations of sufficient quantity and quality at all four measurement depths were available at 21 of

the 106 OK Mesonet stations (Fig. 1) and were used to evaluate the Catchment model (section 3b).

3. LDAS

a. Overview

The land surface model used in LDAS and in this study is the Catchment land surface model (Koster et al. 2000). The Catchment model is a nontraditional modeling framework that includes an explicit treatment of subgrid soil moisture variability and its effect on runoff and evaporation. The basic computational unit of the model is the watershed, whose boundaries are defined by topography. Within each element, the vertical profile of soil moisture is given by the equilibrium soil moisture profile and the deviations from the equilibrium profile in a 1-m root zone layer and in a 2-cm surface layer. Moreover, the model describes the horizontal redistribution of soil moisture (based on the statistics of the catchment topography) in each watershed. The soil and vegetation parameters used in the Catchment model are from the NASA Goddard Earth Observing System, version 5 (GEOS-5) global modeling system (Rienecker et al. 2008).

In a data assimilation system, the model-generated soil moisture is corrected toward the observational estimate. The LDAS data assimilation system is based on the ensemble Kalman filter (EnKF) and dynamically updates model error covariance information by producing an ensemble of model predictions, which are individual model realizations perturbed by the assumed model error (Reichle et al. 2007). The ensemble approach is widely used in hydrologic data assimilation because of its flexibility with respect to the type of model error (Crow and Wood 2003) and is well suited to the nonlinear character of land surface processes (Reichle et al. 2002a,b). As already mentioned, the accurate specification of model and observation errors is the key to successful data assimilation (Reichle et al. 2008). Here, we focus on the ability of the modeling system to characterize precipitation and soil moisture errors without actually assimilating soil moisture observations into the land surface model.

b. Evaluation of model soil moisture

Our study of the rainfall error models depends in part on the ability of the Catchment model to describe soil moisture dynamics in a realistic manner. Numerous studies have demonstrated the Catchment model's viability for large-scale soil moisture modeling (Reichle et al. 2009; Bowling et al. 2003; Nijssen et al. 2003; Boone et al. 2004). For further demonstration, this section compares soil moisture time series from OK Mesonet station observations and corresponding Catchment model simulations, generated by forcing the model with WSR-88D rainfall and GLDAS meteorological forcing fields. The model was spun up by looping 3 times over the 3 yr of forcing data.

In situ soil moisture measurements and output from land surface models designed for global simulations (such as the Catchment model) typically exhibit systematic differences in their estimates of soil moisture (Reichle et al. 2004). These systematic differences are, among other reasons, related to (i) the point-scale character of the in situ observations versus the distributed nature of the model estimates and (ii) a mismatch in the available measurement depths and the vertical resolution of the land surface model. Regarding the latter point, *surface* soil moisture hereafter refers to the OK Mesonet soil moisture measured at 5-cm depth and the 0–2-cm surface soil moisture output from the Catchment model. The *root zone* soil moisture is defined here as the 0–100-cm output from the Catchment model and the corresponding depth-weighted average over the 5-, 25-, 60-, and 75-cm OK Mesonet observations (with weights of 0.15, 0.27, 0.25, and 0.33, respectively).

In global soil moisture modeling and data assimilation the systematic differences can be addressed through rescaling or bias estimation (Reichle et al. 2007; De Lannoy et al. 2007). Here, we focus on anomaly time series, specifically standard-normal deviates that capture the phase correspondence between model estimates and in situ measurements, regardless of potential mean biases or differences in dynamic range (Entekhabi et al. 2010b). Figure 2 shows standard-normal deviate daily time series of (i) model-predicted surface and root zone soil moisture, and (ii) corresponding Mesonet observations during the three summer seasons [months of June, July, August, and September (JJAS)] of 2004, 2005, and 2006. The standard-normal deviates shown in Fig. 2 are computed by subtracting the 2004–06 JJAS mean and dividing by the corresponding standard deviation. Two representative Mesonet stations (one in the wetter eastern half and one in the drier western half of the region) and the corresponding 25-km gridcell model simulations were selected to show standard-normal deviate time series. A station-average standard-normal deviate time series is also computed across the 21 good-quality Mesonet stations and the corresponding 25-km grid cells where sufficient OK Mesonet observations were available for all four measurement depths.

Figure 2 demonstrates that the standard-normal deviate time series are consistent between surface and root zone soil moisture, and that the variations of the Catchment model soil moisture are consistent with the OK Mesonet measurements. The correlation coefficients between Mesonet

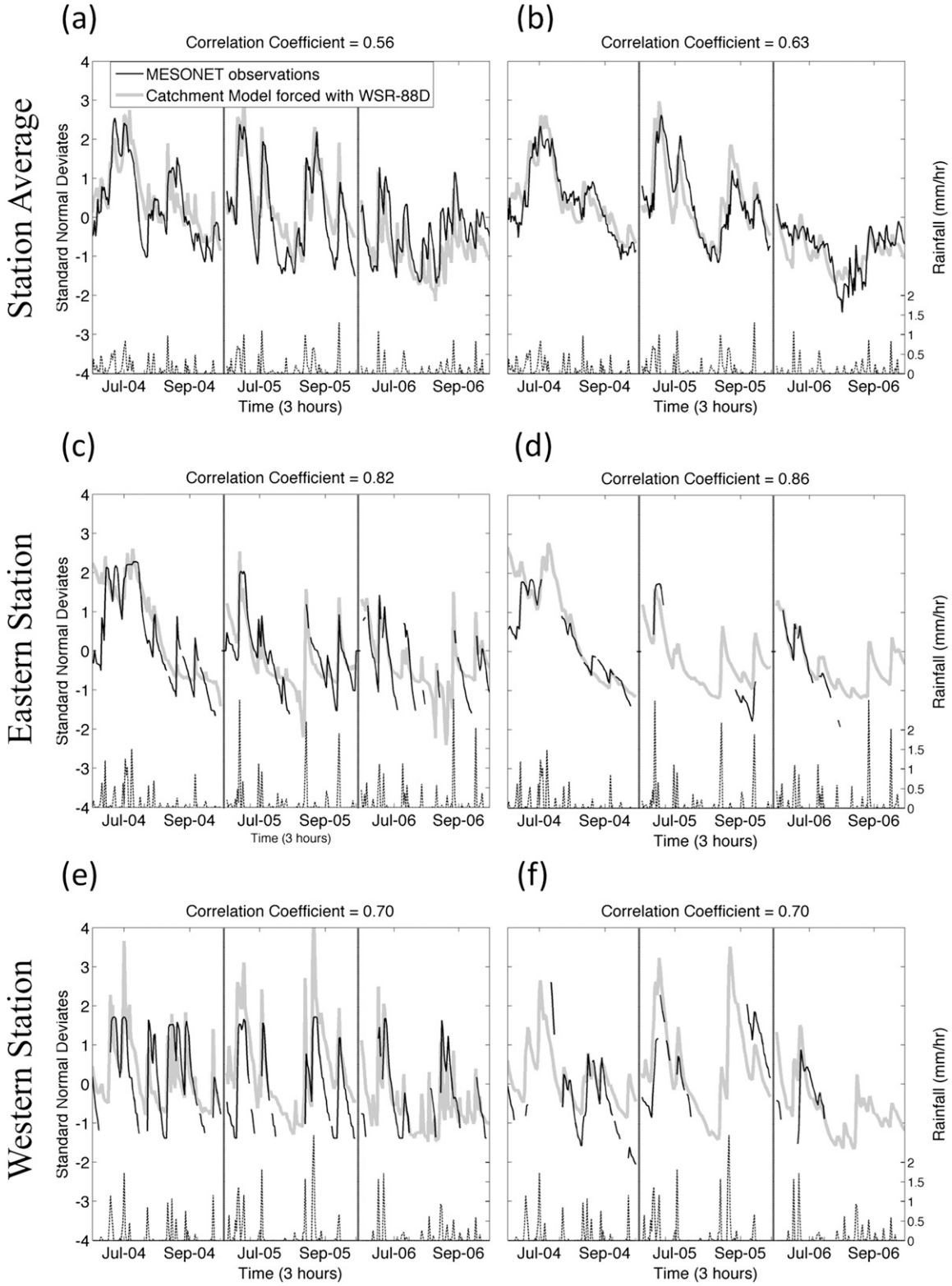

FIG. 2. Standard-normal deviate daily time series of (a),(c),(e) surface and (b),(d),(f) root zone soil moisture for (a),(b) a station average and individual values at the two stations at (c),(d) 36.889°N, 94.845°W and (e),(f) 35.842°N, 98.526°W. Corresponding WSR-88D rainfall time series are also shown. Summer (June–September) time series are shown for 2004–06 and are separated by a vertical line in the plots.

and Catchment model soil moisture across the 21 stations are 0.56 for surface soil moisture and 0.63 for root zone soil moisture. For the individual stations shown in Figs. 2 the correlation coefficients are 0.82 (0.86) for the surface soil moisture (root zone soil moisture) at the eastern station and 0.70 (0.70) for the western location. The root zone soil moisture variations are smoother than those of surface soil moisture because the upper few centimeters of the soil are more exposed to the atmosphere and vary more rapidly in moisture content in response to rainfall forcing and evaporation. Based on this analysis, we are confident of the viability of the soil moisture modeling system for use in this study.

4. The rainfall error models

a. Overview

The objective of the study is to contrast the LDAS rainfall error model with the more complex SREM2D rainfall error model for characterizing rainfall and soil moisture uncertainty. The LDAS model describes rainfall error by scaling the precipitation forcing based on an ensemble of multiplicative perturbation fields that are correlated in space and time (Reichle et al. 2007). This implies that in LDAS all ensemble members agree in terms of rain occurrence and differ only in terms of rainfall-rate magnitude. A spatial correlation structure is imposed based on a two-dimensional Gaussian correlation function. Temporal error correlation is modeled with a first-order autoregressive process in the LDAS error model, but was set to zero in this work for compatibility with the SREM2D implementation. This error structure is parsimonious in its input parameter requirements and is numerically convenient, but it can only approximate the rain-rate error variability, which is not a holistic representation of satellite retrievals that are susceptible to significant rain detection and false detection uncertainties (Hossain and Anagnostou 2006a).

A more inclusive characterization of precipitation uncertainty is based on the Hossain and Anagnostou (2006b) SREM2D rainfall error model. The model was originally developed to use ''reference'' rainfall fields as input that represents the ''true'' surface rainfall, and it employs stochastic space–time formulations to characterize the multidimensional error structure of corresponding satellite retrievals. Reversing in this study the definition of input in SREM2D, the multidimensional structure of deviations from the reference (i.e., radar) rainfall was derived with respect to the satellite rainfall estimates (input field). This process generates ensembles of radar-like rainfall fields from satellite rainfall retrievals that can be used to force the land surface model, thus generating ensembles of model-predicted soil moisture fields. This approach is although similar to the LDAS scheme, allows more complexity in the error modeling structure of rainfall.

Again, the precipitation error in the LDAS model assumes a perfect delineation of rainy and nonrainy areas and simply scales the input precipitation forcing with a multiplicative perturbation (different scaling factor for each time, location, and ensemble member). This implies, for example, that all LDAS ensemble members have zero precipitation whenever the input precipitation is zero. In SREM2D ensemble members, by contrast, rain can occur in areas where the input precipitation is zero. Specifically, the joint spatial probability of successful delineation of rainy and nonrainy areas is characterized in SREM2D using Bernoulli trials of a uniform distribution with a correlated structure generated based on Gaussian random fields. These Gaussian random fields are transformed into uniform distribution random fields via an error function transformation. For additional details on SREM2D we refer the reader to Hossain and Anagnostou (2006b).

Modeling the spatial structures for detection is an important element of SREM2D as real sensor data are known to exhibit spatial clusters for false rain and false no-rain detection. In summary, the key difference between the two error models is that SREM2D characterizes the spatial structure of the successful delineation of rainy and nonrainy areas, while both models describe the spatial variability of rain-rate estimation error.

The reference rainfall is defined here as the Stage IV WSR-88D product while the satellite rainfall is the CMORPH global product. For this study, CMORPH rainfall estimates were adjusted to the mean climatology of the radar rainfall to be consistent with the LDAS assumption of unbiased rainfall forcing fields. The bias adjustment factor was determined based on the 3-yr time series of WSR-88D and CMORPH rainfall estimates over Oklahoma. Figure 3 illustrates the consistency in the cumulative area-average precipitation during the study period between the radar precipitation and the adjusted CMORPH precipitation.

The input parameters for the SREM2D and LDAS precipitation error models are summarized in Table 1. In both error models, we set the mean value for the lognormal multiplicative perturbations to unity to obtain (nearly) unbiased replicates. The remaining parameters were calibrated to obtain replicates of the CMORPH precipitation that reproduce the overall standard deviation of the CMORPH versus radar rainfall errors (as will be demonstrated below in Table 2). From Table 1 we note that the standard deviation parameter value for multiplicative perturbations is 0.2 for SREM2D and 0.4 for LDAS. The SREM2D parameter is smaller because

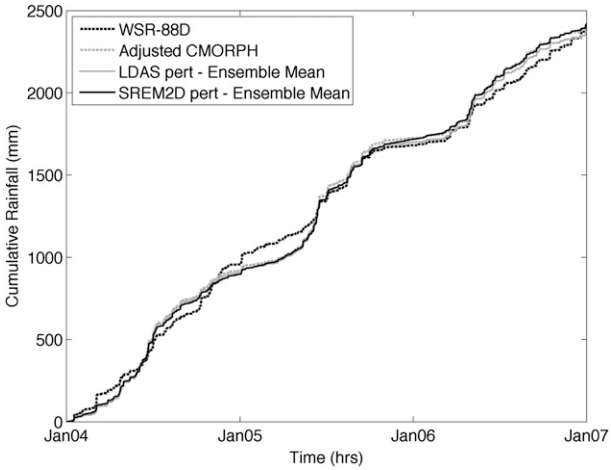

FIG. 3. Cumulative hyetograph during the study period (2004–06) of the WSR-88D dataset, the satellite dataset (adjusted CMORPH), and the mean of ensembles produced by perturbing the adjusted CMORPH rainfall with the LDAS error model (LDAS pert) and SREM2D (SREM2D pert).

in the more complex SREM2D, variability is added from additional sources (e.g., rain detection and false detection uncertainties), whereas in LDAS the uncertainty is entirely determined by the multiplicative perturbations. As stated above, time correlation was not applied in this study. Error correlation lengths for the multiplicative error (SREM2D and LDAS) and for the delineation of rainy and nonrainy areas (SREM2D only) range from 70 to 190 km (Table 1). Additional SREM2D parameters include a lookup table for the probability of successful rain detection (not shown in Table 1).

b. *Performance of the rainfall error models*

Before we analyze the performance of the SREM2D and LDAS error models in terms of the error statistics of the generated ensemble rainfall fields, it is instructive to discuss sample realizations of the precipitation replicates. Figure 4 shows snapshots (for three consecutive time steps) of a precipitation event from radar and satellite, along with one representative member each from the LDAS and SREM2D ensembles. Generally, the structure of the radar (reference) rainfall is well captured by the satellite as well as by the perturbed fields. By design, each LDAS ensemble member is only a rescaled version of the satellite rain field (with spatially distributed scaling factors). In contrast, SREM2D may introduce rain in pixels where the satellite does not measure rain (to statistically represent the rain detection error) while it may assign zero to pixels where the satellite detects rain (to statistically represent the false detection error). This is due to parameterizations in SREM2D that describe the probability of detection and false alarms as a function

TABLE 1. Error model parameters.

	Units	LDAS	SREM2D
Mean of lognormal multiplicative error	Dimensionless	1.00	1.00
Std dev of lognormal multiplicative error	Dimensionless	0.40	0.20
False alarm mean rain rate	mm h^{-1}	n/a	0.24
No-rain probability of detection	Dimensionless	n/a	0.96
Correlation length for multiplicative error	km	90	90
Correlation length for successful rain detection	km	n/a	190
Correlation length for successful no-rain detection	km	n/a	70

of satellite rainfall. This is apparent in the top panelsof Fig. 4, where the SREM2D replicate introduces precipitation in the southwestern quadrant of the domain, where no rain was estimated by CMORPH. During the second 3-h time step (middle row of Fig. 4) the SREM2D ensemble member shows a dry area in the southeastern corner of the domain (which corresponds to a dry region in the radar measurement), while the satellite detects rain in those pixels (false alarm case). The same effect can be observed in the last snapshot (bottom row of Fig. 4), where a dry area along the western border of the domain is well captured by the SREM2D perturbed field, even though CMORPH erroneously detected rain. Note that the perturbed LDAS and SREM2D fields in Fig. 4 are just one ensemble member: they are not meant to replicate the true field, but rather to illustrate the statistical properties of the ensemble.

The generated ensemble fields are also assessed in terms of the first- (mean) and second-order (variance) error statistics against the reference (radar) and contrasted to the same statistics determined for the adjusted CMORPH satellite dataset. Three spatial scales are considered—100 km (8 grid cells), 50 km (55 grid cells), and 25 km (220 grid cells)—to assess how the error modeling techniques can represent the mean and variance of satellite error across scales. Results are presented in Table 2. The error is here defined as the

TABLE 2. Mean and std dev of rainfall error (difference between satellite–ensembles and radar in mm h^{-1}) conditional to radar or satellite being > 0.

	25 km		50 km		100 km	
Spatial scale	Mean	Std dev	Mean	Std dev	Mean	Std dev
Adjusted CMORPH	0.00	1.09	0.00	0.82	0.00	0.55
LDAS realizations	−0.01	1.19	−0.01	0.90	−0.01	0.61
SREM2D realizations	0.00	1.14	0.00	0.84	0.00	0.56

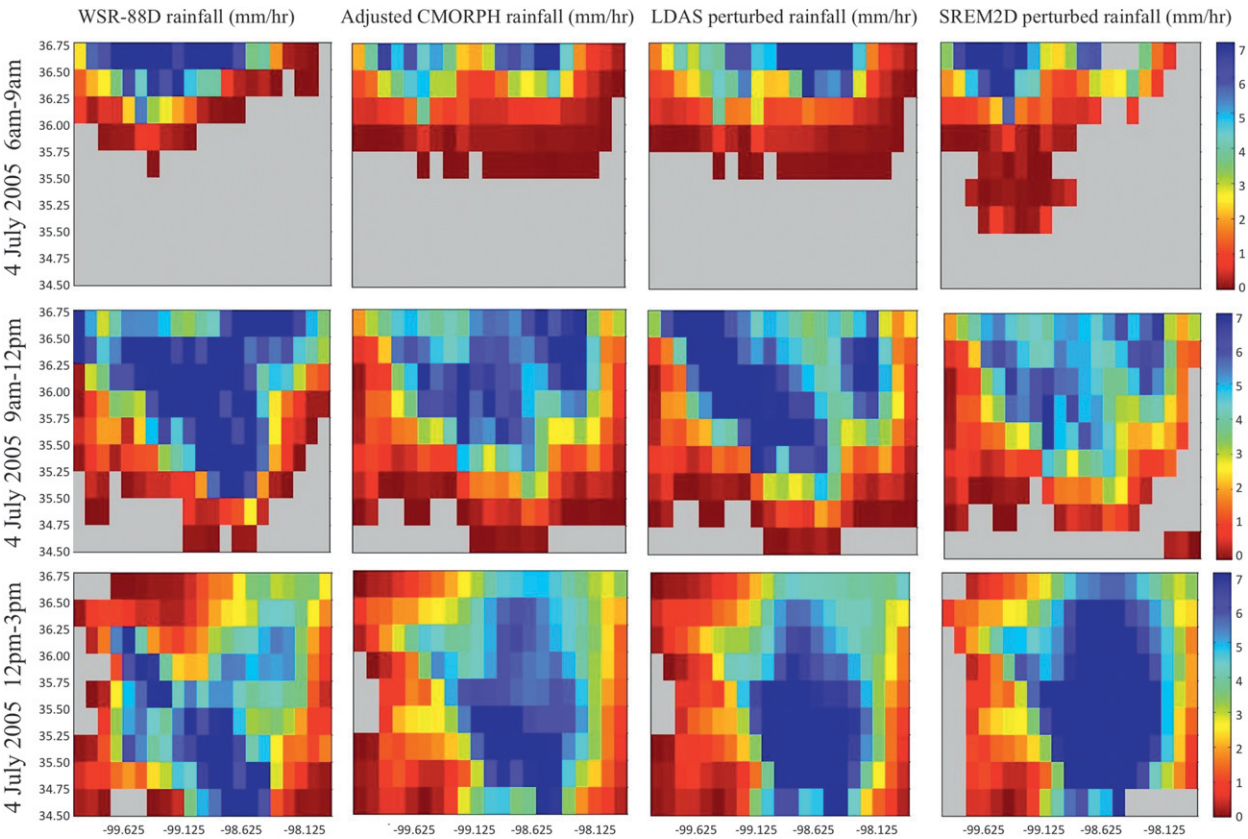

FIG. 4. Rainfall maps for the event of 4 Jul 2005 for the three time steps: (top to bottom) 0600–0900, 0900–1200, and 1200–1500 local time (LT).

difference at 3-h time steps between the adjusted CMORPH satellite rainfall (or LDAS ensemble member, or SREM2D ensemble member) and the reference radar rainfall. In the case of perturbed rainfall fields, the values reported in the table are the average of the error statistics (mean and standard deviation) across the individual ensemble members.

The bias values shown in Table 2 are negligible across all scales because we adjusted the CMORPH precipitation to match the 3-yr total radar precipitation (see Fig. 3 and discussion above), and because the perturbations generated by both precipitation error models are designed to be unbiased, which is also illustrated in Fig. 3. Moreover, the error standard deviation decreases with increasing scale and is well represented by both error models. This suggests that after calibration the two error schemes can adequately capture the magnitude of the rainfall error, which is consistent with the results of Hossain and Anagnostou (2006a).

5. The soil moisture simulation experiments

The Catchment model was forced with perturbed and unperturbed precipitation fields to generate soil moisture fields in two different modes: simulation and open loop runs, which are described next and schematized in Fig. 5. All Catchment model integrations were initialized from a spinup simulation conducted with the WSR-88D radar precipitation (section 2a).

a. Simulation mode—No precipitation perturbations

As shown in the center and left portions of Fig. 5, the WSR-88D (radar) and unperturbed, adjusted CMORPH (satellite) rainfall fields force the Catchment model to generate surface and root zone soil moisture fields. The soil moisture output from the model integration forced with the radar rainfall represents the reference for soil moisture. Soil moisture modeling errors are then computed by differencing the soil moisture estimates derived from CMORPH and the reference soil moisture. Alternatively, in situ soil moisture observations from the OK Mesonet could be considered as the reference. However, the problem with using the in situ data in the subsequent soil moisture error investigation is that the effect of rainfall error could not be isolated from other error sources. This would make it difficult to study the significance of precipitation error model complexity in characterizing the predictive uncertainty of soil moisture.

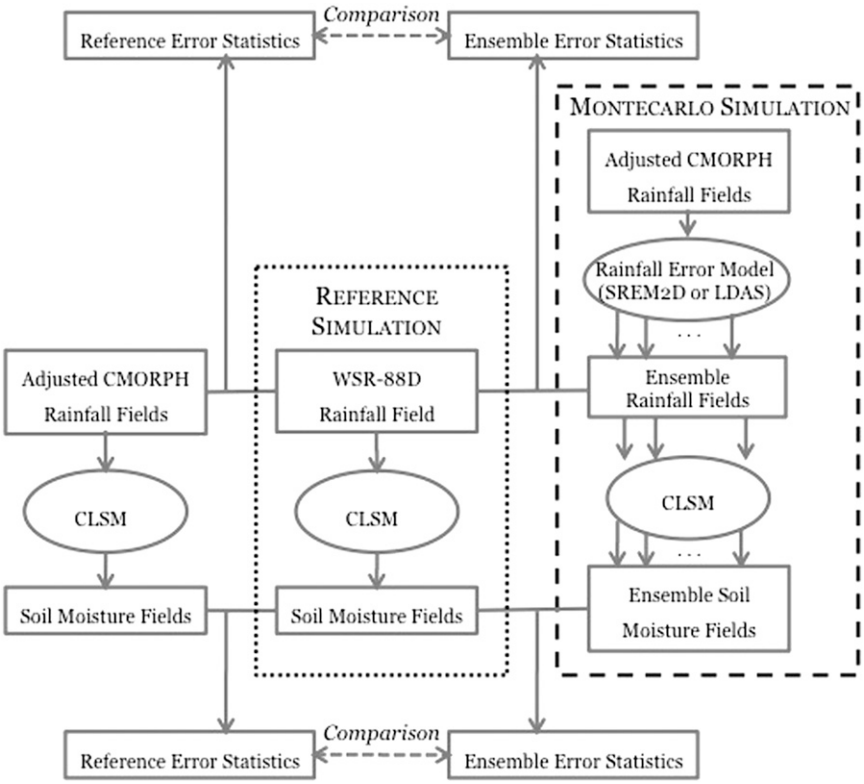

FIG. 5. Experiment setup of the error propagation study.

b. *Ensemble mode with precipitation perturbations*

Ensemble runs are Monte Carlo simulations as shown in the rightmost box in Fig. 5. The adjusted CMORPH satellite precipitation fields were perturbed using the SREM2D and, separately, the LDAS rainfall error model, to force the Catchment model. Each ensemble integration consists of 24 members and generates an ensemble of soil moisture fields. Each ensemble integration is then evaluated against the reference soil moisture fields obtained from the simulation experiments (without precipitation perturbations) in terms of error statistics. Put differently, we analyze the skill of the LDAS and SREM2D ensemble integrations to represent the soil moisture modeling error with respect to the reference fields.

6. Results and discussion

a. *Rainfall to soil moisture error propagation*

Figures 6, 7, and 8 illustrate time series of 0–2-cm surface soil moisture and 0–100-cm root zone soil moisture from the Catchment model forced with the unperturbed (reference) radar rainfall (thick lines), the unperturbed satellite precipitation (thin lines), and the LDAS and SREM2D perturbed rainfall (ensemble envelopes shown in gray shading). Time series are shown for a representative interval of four warm-season months (June–September 2005). Two different spatial scales are considered: the average over the whole domain (Fig. 6) and the 25-km gridcell resolution (Figs. 7 and 8). For the latter, two representative grid cells have been selected—one in the eastern half (representing wetter conditions) and the other in the western half of the region (representing drier conditions).

As expected, the domain-average soil moisture time series (Fig. 6) show less variability than the corresponding time series at the 25-km scale (Figs. 7 and 8), with a commensurately smaller ensemble spread. Figure 6 indicates little difference between the SREM2D and LDAS ensemble integrations at the domain-average scale, both in terms of the rainfall and the soil moisture time series. At the 25-km scale (Figs. 7 and 8), however, the ensemble envelope of SREM2D is wider than that of LDAS and better encapsulates the radar-measured rainfall because the SREM2D rainfall error model generates more variability. This behavior is evident in both surface and root zone soil moisture time series, which show similar ensemble envelopes for both depths.

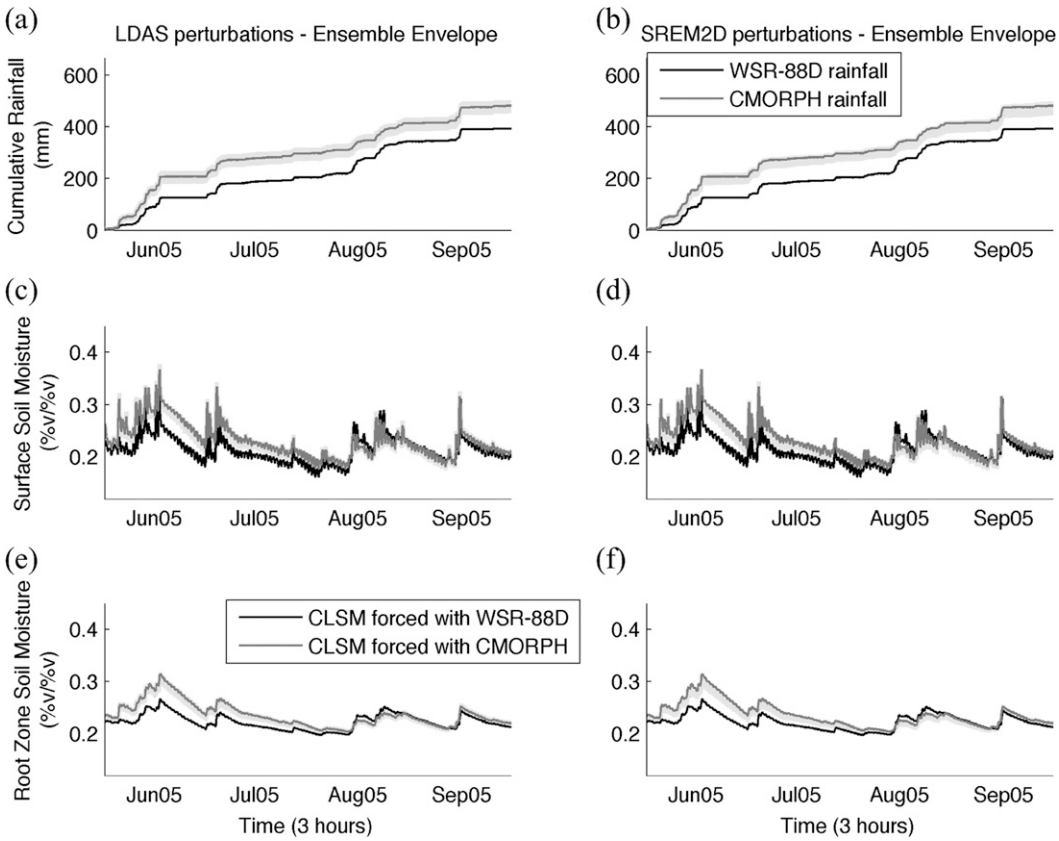

FIG. 6. Representative 4-month (Jun–Sep 2005) time series of (a),(b) cumulative rainfall, (c),(d) surface soil moisture, and (e),(f) root zone soil moisture domain average. Results shown are from (a),(c),(e) LDAS error model and (b),(d),(f) SREM2D.

b. *Exceedance and uncertainty ratios*

The wider ensemble envelopes of the SREM2D ensemble increase the probability of encapsulating the reference simulations between the lower and upper ensemble bounds of the ensemble. In this section we present two metrics, the exceedance ratio (ER) and the uncertainty ratio (UR), that further quantify the ability of the ensemble integrations to capture precipitation and soil moisture errors. The exceedance ratio measures the potential of the error model to capture the observed fields, while the UR provides information about the relative predictive capability, specifically, the ratio of the ensemble spread relative to a reference value. Each metric is computed for the perturbed rainfall (or soil moisture) with respect to the radar rainfall (or radar rainfall–forced soil moisture). Two contrasting issues are considered in using these statistics: if the uncertainty limits are too narrow (i.e., ER is high), then the comparison with the reference fields suggests that the model errors are underestimated; on the other hand, if the limits are too wide (i.e., UR is high), the model may not have an adequate predictive capability (Hossain et al. 2004).

Specifically, the exceedance ratio is defined as

$$\mathrm{ER} = \frac{N_{\mathrm{exceedance}}}{N_t}, \tag{1}$$

where $N_{\mathrm{exceedance}}$ is the number of times the reference rainfall (or reference-derived soil moisture) falls outside the ensemble envelope and N_t is the total number of times and locations. The uncertainty ratio is defined as the ratio of the simulated uncertainty (defined as the average difference between the upper and lower limits of the ensemble envelope) normalized by the corresponding reference variable (defined as the average precipitation or soil moisture):

$$\mathrm{UR} = \frac{\sum_{i=1}^{N_t} (\hat{\vartheta}^i_{\mathrm{upperlim}} - \hat{\vartheta}^i_{\mathrm{lowerlim}})}{\sum_{i=1}^{N_i} \vartheta^i}. \tag{2}$$

In other words, UR represents the bulk variability in the perturbed variable relative to the typical value of that variable (Hossain and Anagnostou 2005).

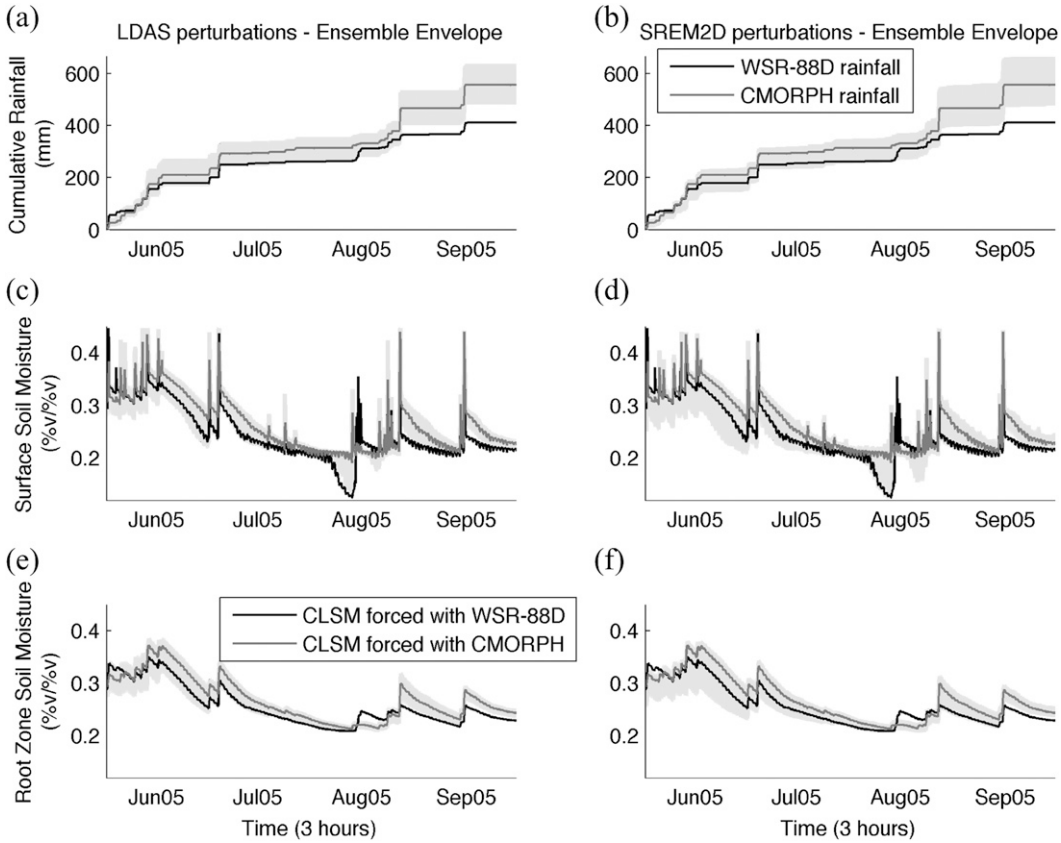

FIG. 7. Representative 4-month (Jun–Sep 2005) time series of (a),(b) cumulative rainfall, (c),(d) surface soil moisture, and (e),(f) root zone soil moisture at a 25-km grid cell in the eastern half of the region. Results shown are from (a),(c),(e) LDAS error model and (b),(d),(f) SREM2D.

The statistics presented above were calculated for different spatial scales (25, 50, and 100 km). The leftmost panels of Fig. 9 show that, for precipitation, ER assumes considerably higher values in the LDAS error model compared to SREM2D. Specifically, in the best case—at the 25-km scale—the radar rainfall measurement is included in the envelope of the LDAS realizations only 80% of the time on average. This percentage reduces to a value lower than 70% at coarser resolutions. On the other hand, in the case of SREM2D, about 95% of the time the reference precipitation is between the minimum and the maximum value of the ensemble at all spatial scales. The difference between the two error models is due to the SREM2D potential of producing rain even where the input precipitation is zero, and of assigning no rain to areas where the reference measures precipitation. The scale dependence in the ER values of LDAS is attributed to the fact that this error model does not account for rain detection uncertainties that may introduce biases at coarser scales. As expected, the UR exhibits lower values in the case of LDAS error model relative to SREM2D, confirming that the more complex SREM2D generates higher variability than the LDAS approach.

The center and rightmost panels of Fig. 9 show the ER and UR metrics for soil moisture estimates from the Catchment model. Values of ER are considerably higher in soil moisture compared to precipitation, indicating that the output from both ensemble integrations generally captures soil moisture error variability less definitively than rainfall error. Again, the uncertainty structure is similar for surface and root zone soil moisture, with comparable ER values. UR is slightly lower for root zone than for surface soil moisture because deeper soil moisture carries less variability, as already discussed. Similar to what was shown for precipitation, SREM2D-derived soil moisture fields have higher potential (40% at the 25-km scale) of enveloping reference fields than those derived by the LDAS error propagation scheme (30% at the 25-km scale). The downside of producing more variability is that the ensemble spread could be overestimated, which could result in excessive weight given to the observations in ensemble-based data assimilation.

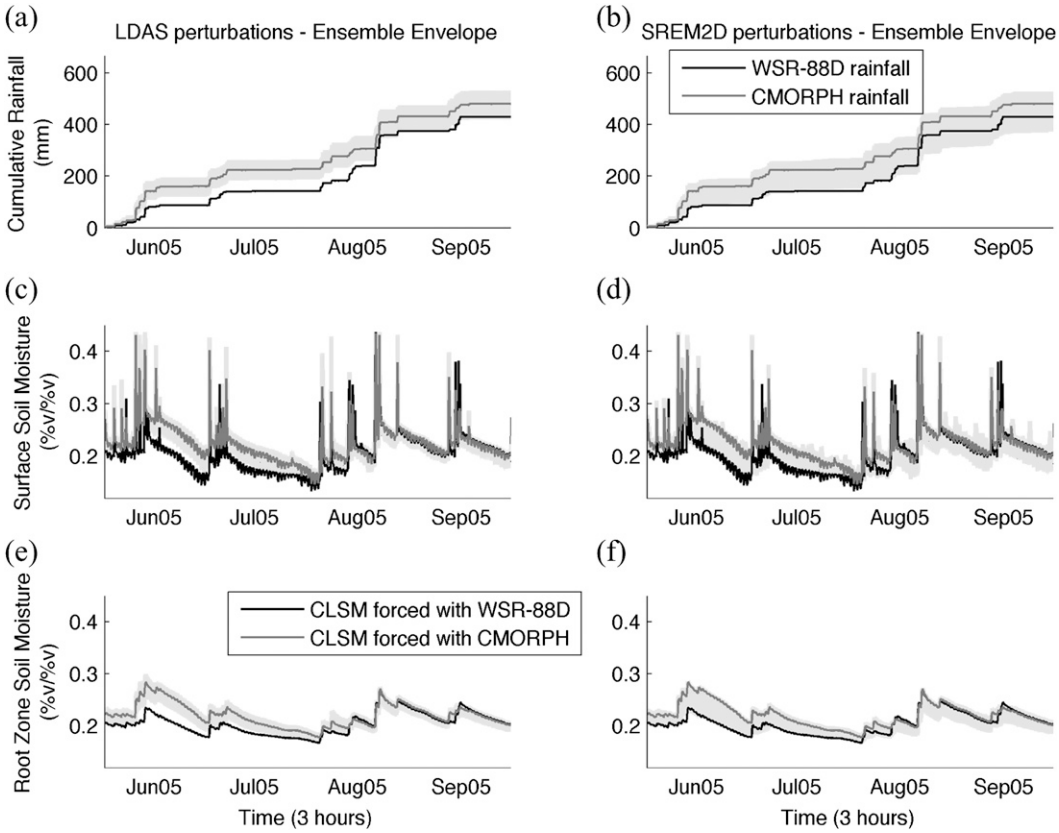

FIG. 8. Same as Fig. 7 but in the western half of the region.

In the propagation from rainfall to soil moisture, the exceedance ratio is amplified: while ER is close to 0.05 for precipitation fields, ER reaches values of 0.65 on average for soil moisture (Fig. 9). In contrast, the uncertainty ratio drops considerably in the propagation from precipitation to soil moisture: UR values for precipitation replicates range from 1 to 4, while UR values for soil moisture replicates are only 0.05–0.15. This dampening of the variability of the error is due to two effects: the integration of highly intermittent precipitation into more smoothly varying soil moisture, and the natural lower and upper bounds of soil moisture relative to rainfall. Figure 9 thus clearly demonstrates that soil moisture error variability is attenuated in the rainfall to soil moisture transformation process in a nonlinear fashion.

In summary, the difference between the SREM2D and LDAS error models that was evident in terms of rainfall reduces considerably when the simulated soil moisture fields are considered (Fig. 9). Perturbing precipitation with a more complex precipitation error approach leads to only slightly higher variability in the simulated soil moisture fields and only a moderate increase of the potential of enveloping the reference. This suggests that the sensitivity of soil moisture data assimilation to the choice of precipitation error model may be limited.

c. *Relative bias and relative root-mean-square error*

To further highlight the features of the rain error models and the propagation of error statistics from precipitation to soil moisture we now present two additional error metrics: the relative bias (rBIAS) and relative root-mean-square error (rRMSE). Specifically, we first compute reference values for these two statistics that measure the errors between the unperturbed (adjusted) CMORPH precipitation (or corresponding soil moisture fields) and the reference WSR-88D radar precipitation (or corresponding soil moisture fields). These reference statistics, shown with dots in Fig. 10, are defined as follows:

$$\mathrm{rBIAS} = \frac{\sum_{k=1}^{N}(\hat{\vartheta}_k - \vartheta_k)}{\sum_{k=1}^{N}\left(\frac{\hat{\vartheta}_k + \vartheta_k}{2}\right)} \quad \text{and} \tag{3}$$

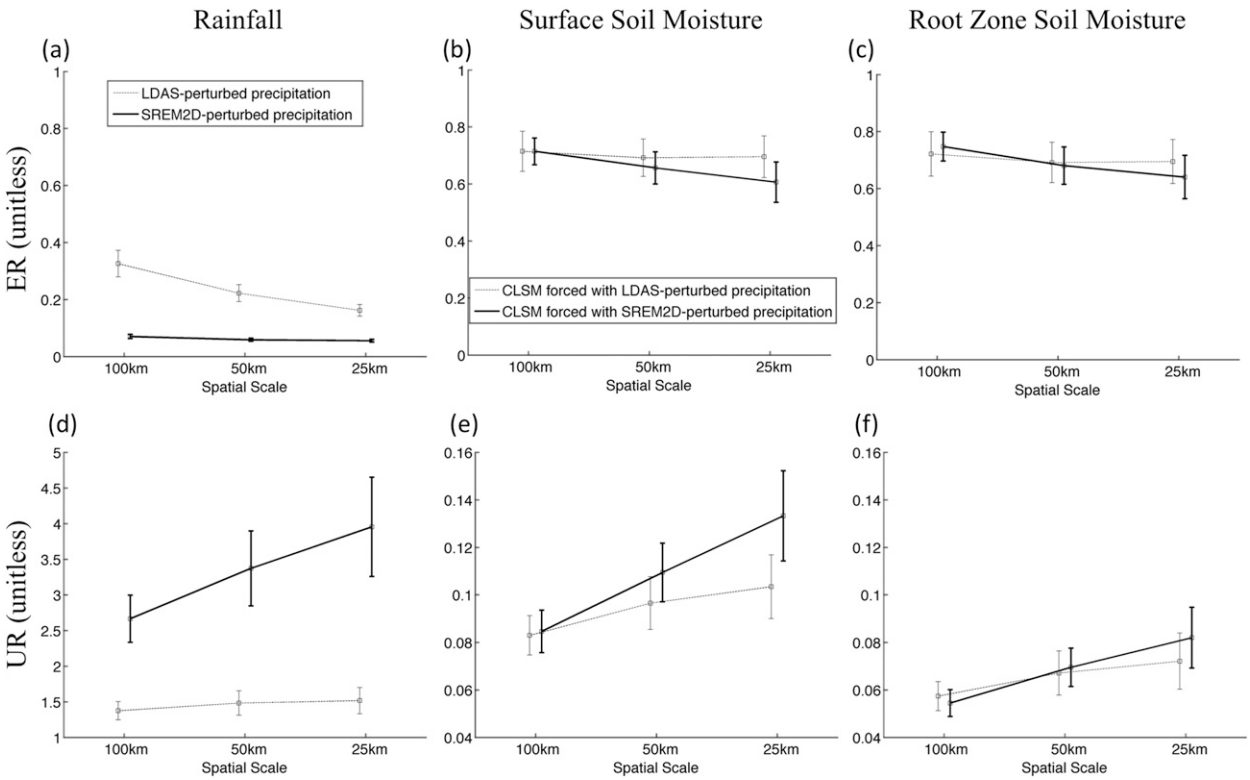

FIG. 9. (a)–(c) ER and (d)–(f) UR for (a),(d) rainfall, (b),(e) surface soil moisture, and (c),(f) root zone soil moisture determined at three scales of aggregation. The plotted point with vertical bars indicate the ensemble mean and 1 std dev of the ER and UR values. Scales differ between the precipitation UR and soil moisture UR.

$$\mathrm{rRMSE} = \frac{\sqrt{\frac{1}{N}\sum_{k=1}^{N}(\hat{\vartheta}_k - \vartheta_k)^2}}{\mathrm{std}(\vartheta_k)}, \tag{4}$$

where N = total number of time steps $\times$ total number of grid cells, $\hat{\vartheta}$ represents CMORPH precipitation (or corresponding soil moisture fields), and ϑ is the reference WSR-88D radar precipitation (or corresponding soil moisture fields).

Next, we compute the same statistics for each individual member of the LDAS (or SREM2D) ensemble for precipitation and soil moisture (again versus the reference radar precipitation or corresponding reference soil moisture). In Eqs. (3) and (4), $\hat{\vartheta}$ can then be read as precipitation (or soil moisture) from a single member of the LDAS (or SREM2D) ensemble. The rBIAS and rRMSE metrics for the individual ensemble members are then averaged across the ensemble, separately for SREM2D and LDAS (shown in Fig. 10 as squares), and can be compared to the reference statistics. Ideally, the statistics calculated for the ensemble members should replicate, at least on average, the reference error statistics. The metrics described in this section differ from the ones shown in Table 2; here we are computing relative (unitless) statistics, while Table 2 presents the mean and the standard deviation of the errors.

Figure 10 shows that, broadly speaking, both rainfall error models yield similar rBIAS and rRMSE values, and that both error models adequately reproduce the reference statistics. A closer inspection of the rBIAS values for precipitation reveals a small residual bias in LDAS perturbed precipitation. Furthermore, the absolute value of rBIAS for soil moisture is slightly larger than that for rainfall, which again suggests that the precipitation to soil moisture error transformation is nonlinear. On the other hand, the relative RMSE is appreciably smaller for soil moisture than for precipitation, which confirms what was shown in the uncertainty ratios and again reflects the integrating nature of the soil moisture. Together, these statistics illustrate the nonlinear transformation of precipitation error that introduces biases in soil moisture simulations, while dampening error variability. This corroborates our observation in the previous section that simulated soil moisture ensembles are less sensitive to the complexity of the precipitation error structure than precipitation ensembles themselves.

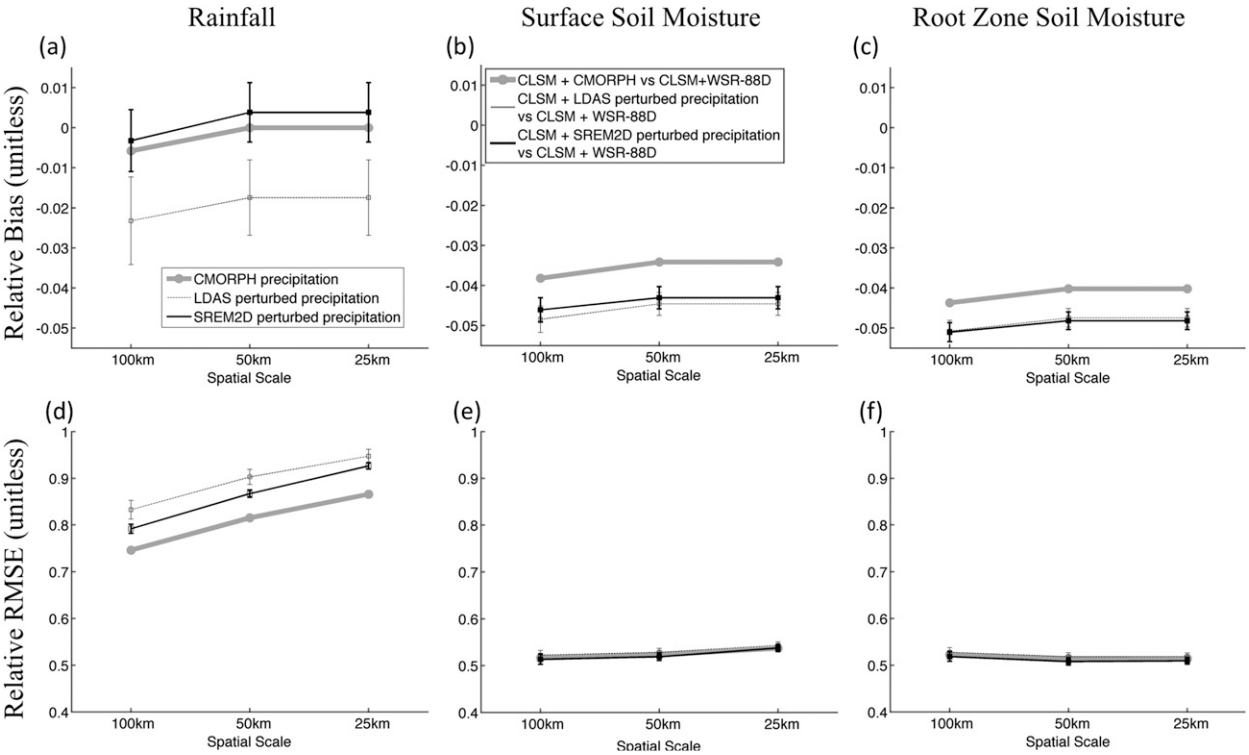

FIG. 10. Error statistics of rainfall of adjusted CMORPH and of ensemble fields perturbed by LDAS and SREM2D models with respect to the reference (WSR-88D) rainfall: (a) rBIAS and (d) rRMSE. (b),(e) As in (a),(d), but for surface soil moisture simulated by the CLSM forced with adjusted CMORPH precipitation and ensemble rainfall perturbed by LDAS and SREM2D with respect to soil moisture simulated by CLSM forced with reference (WSR-88D) precipitation fields. (c),(f) As in (b),(e), but for root zone soil moisture. Error bars indicate the std dev of the metric across the ensemble.

7. Conclusions

This study focused on the sensitivity of soil moisture errors to rainfall error modeling of different complexity within the LDAS developed at the NASA GMAO. The simpler LDAS rainfall error model was contrasted with the more complex SREM2D rainfall error scheme, which accounts for actual satellite rainfall error characteristics, such as probability of detection and probability of false alarm. We find that SREM2D provides more uncertainty in the precipitation ensemble and better encapsulates the reference precipitation (WSR-88D dataset). Generally, the SREM2D ensemble reproduces the reference error statistics (relative bias and relative RMSE) better than the LDAS error ensemble (Fig. 10).

Soil moisture simulations are shown to be less sensitive to the complexity of the precipitation error modeling approach than the precipitation fields themselves because of the dampening of the error variability along with a nonlinear increase of the mean error. This can be attributed to different factors: (i) the rain to soil moisture error propagation is a nonlinear and integrating process, and (ii) soil moisture dynamics are inherently dissipative (i.e., perturbations are damped in time), reducing the apparent sensitivity of soil moisture relative to precipitation.

The higher variability added by SREM2D to the precipitation ensemble has little effect on soil moisture simulations. The ensemble produced by perturbing the forcing precipitation with a more complex precipitation error approach leads to only a slightly higher potential of enveloping the reference modeled soil moisture.

One caveat to our results is that we tested the precipitation to soil moisture propagation of errors only with the Catchment land surface model. Future studies should investigate the sensitivity to different approaches for land surface modeling. Nevertheless, we are confident that our general conclusions remain valid if other land surface models are substituted for the Catchment model, even if some details of the error statistics are likely to change. Note also that this work was done with a view toward land data assimilation at the global scale, for which the Catchment model has been used successfully (Reichle et al. 2007).

When used in stand-alone mode, both precipitation error models investigated here include the option

of generating precipitation replicates that are subject to temporally correlated errors. Such temporal error correlations were not used here because their use would have made the integration of SREM2D into the LDAS far more difficult, and thus were left for future work. It is possible that the addition of temporal error correlations increases the ability of the LDAS error model to generate precipitation replicates with enhanced variability and thus reduces its exceedance ratio, bringing it more in line with that of SREM2D-generated replicates.

Our results suggest future studies on how SREM2D can be employed to improve the use of remotely sensed data in a land data assimilation system. Such studies should focus on understanding and quantifying the impact of precipitation error modeling on the efficiency of assimilating soil moisture fields in a land data assimilation system.

Finally, the results obtained from this study provide useful information about the use of satellite rainfall observations to model hydrologic processes, thus providing valuable feedback for future hydrologic missions, including the NASA Global Precipitation Measurement Mission (http://gpm.gsfc.nasa.gov) and the NASA Soil Moisture Active Passive Mission (http://smap.jpl.nasa.gov; Entekhabi et al. 2010a). The results also aid the development or implementation of satellite rainfall observations into land data assimilation systems.

Acknowledgments. V. Maggioni was supported by a NASA Earth System Science Graduate Fellowship. R. Reichle was supported by NASA Grant NNX08AH36G. E. Anagnostou was supported by NASA Grant NNX07AE31G. Computing was supported by the NASA High End Computing Program. The authors thank Faisal Hossain from the Tennessee Technological University for his precious help with the SREM2D model.

REFERENCES

Anagnostou, E. N., V. Maggioni, E. I. Nikolopoulos, T. Meskele, F. Hossain, and A. Papadopoulos, 2010: Benchmarking high-resolution global satellite rainfall products to radar and rain gauge rainfall estimates. *IEEE Trans. Geosci. Remote Sens.,* **48,** 1667–1683.

Bellerby, T., and J. Sun, 2005: Probabilistic and ensemble representations of the uncertainty in IR/microwave rainfall product. *J. Hydrometeor.,* **6,** 1032–1044.

Betts, A. K., and J. H. Ball, 1998: FIFE surface climate and site-average dataset 1987–89. *J. Atmos. Sci.,* **55,** 1091–1108.

Bloom, S., and Coauthors, 2005: Documentation and validation of the Goddard Earth Observing System (GEOS) Data Assimilation System: Version 4. Vol. 26, Series on Global Modeling Data Assimilation Tech. Rep. 104606, 187 pp. [Available from Global Modeling and Assimilation Office, NASA Goddard Space Flight Center, Greenbelt, MD 20771.]

Boone, A., and Coauthors, 2004: The Rhone aggregation land surface scheme intercomparison project: An overview. *J. Climate,* **17,** 187–208.

Bowling, L. C., and Coauthors, 2003: Simulation of high latitude hydrological processes in the Torne–Kalix basin: PILPS Phase 2(e) 1: Experiment description and summary intercomparisons. *Global Planet. Change,* **38,** 1–30.

Brock, F. V., K. C. Crawford, R. L. Elliott, G. W. Cuperus, S. J. Stadler, H. L. Johnson, and M. D. Eilts, 1995: The Oklahoma Mesonet: A technical overview. *J. Atmos. Oceanic Technol.,* **12,** 5–19.

Carpenter, T. M., J. A. Sperfslage, K. P. Georgakakos, T. Sweeney, and D. L. Fread, 1999: National threshold runoff estimation utilizing GIS in support of operational flash flood warning system. *J. Hydrol.,* **224,** 21–44.

Crow, W. T., and E. F. Wood, 2003: The assimilation of remotely sensed soil brightness temperature imagery into a land surface model using ensemble Kalman filtering: A case study based on ESTAR measurements during SGP97. *Adv. Water Resour.,* **26,** 137–149.

De Lannoy, G. J. M., R. H. Reichle, P. R. Houser, V. R. N. Pauwels, and N. E. C. Verhoest, 2007: Correcting for forecast bias in soil moisture assimilation with the ensemble Kalman filter. *Water Resour. Res.,* **43,** W09410, doi:10.1029/2006WR005449.

Entekhabi, D., and Coauthors, 2010a: The Soil Moisture Active and Passive (SMAP) Mission. *Proc. IEEE,* **98,** 704–716, doi:10.1109/JPROC.2010.2043918.

——, R. H. Reichle, R. D. Koster, and W. T. Crow, 2010b: Performance metrics for soil moisture retrievals and application requirements. *J. Hydrometeor.,* **11,** 832–840.

Fulton, R. A., 1998: WSR-88D Polar-to-HRAP mapping. National Weather Service, Hydrologic Research Laboratory Tech. Memo., 34 pp. [Available online at http://www.nws.noaa.gov/oh/hrl/papers/wsr88d/hrapmap.pdf.]

Hossain, F., and E. N. Anagnostou, 2005: Numerical investigation of the impact of uncertainties in satellite rainfall estimation and land surface model parameters on simulation of soil moisture. *Adv. Water Resour.,* **28,** 1336–1350.

——, and ——, 2006a: Assessment of a multi-dimensional satellite rainfall error model for ensemble generation of satellite rainfall data. *Geosci. Remote Sens. Lett.,* **3,** 419–423.

——, and ——, 2006b: A two-dimensional satellite rainfall error model. *IEEE Trans. Geosci. Remote Sens.,* **44,** 1511–1522.

——, ——, T. Dinku, and M. Borga, 2004: Hydrological model sensitivity to parameter and radar rainfall estimation uncertainty. *Hydrol. Processes,* **18,** 3277–3291.

Jackson, T. J., 1993: Measuring surface soil moisture using passive microwave remote sensing. *Hydrol. Processes,* **7,** 139–152.

Joyce, R. J., J. E. Janowiak, P. A. Arkin, and P. P. Xie, 2004: CMORPH: A method that produces global precipitation estimates from passive microwave and infrared data at high spatial and temporal resolution. *J. Hydrometeor.,* **5,** 487–503.

Koster, R. D., J. Suarez, A. Ducharne, M. Stieglitz, and P. Kumar, 2000: A catchment-based approach to modeling land surface processes in a general circulation model: 1. Model structure. *J. Geophys. Res.,* **105,** 24 809–24 822.

Krajewski, W. F., and Coauthors, 2006: A remote sensing observatory for hydrologic sciences: A genesis for scaling to continental hydrology. *Water Resour. Res.,* **42,** W07301, doi:10.1029/2005WR004435.

Martina, M. L. V., E. Todini, and A. Libralon, 2005: A Bayesian decision approach to rainfall thresholds based flood warning. *Hydrol. Earth Syst. Sci. Discuss.,* **2,** 2663–2706.

Nijssen, B., and Coauthors, 2003: Simulation of high latitude hydrological processes in the Torne–Kalix basin: PILPS Phase 2(e) 2: Comparison of model results with observations. *Global Planet. Change,* **38,** 31–53.

Njoku, E. G., T. J. Jackson, V. Lakshmi, T. K. Chan, and S. V. Nghiem, 2003: Soil moisture retrieval from AMSR-E. *IEEE Trans. Geosci. Remote Sens.,* **41,** 215–229.

Reichle, R. H., D. McLaughlin, and D. Entekhabi, 2002a: Hydrological data assimilation with the ensemble Kalman filter. *Mon. Wea. Rev.,* **130,** 103–114.

——, J. P. Walker, R. D. Koster, and P. R. Houser, 2002b: Extended versus ensemble Kalman filtering for land data assimilation. *J. Hydrometeor.,* **3,** 728–740.

——, R. D. Koster, J. Dong, and A. A. Berg, 2004: Global soil moisture from satellite observations, land surface models, and ground data: Implications for data assimilation. *J. Hydrometeor.,* **5,** 430–442.

——, ——, P. Liu, S. P. P. Mahanama, E. G. Njoku, and M. Owe, 2007: Comparison and assimilation of global soil moisture retrievals from the Advanced Microwave Scanning Radiometer for the Earth Observing System (AMSRE) and the Scanning Multichannel Microwave Radiometer (SMMR). *J. Geophys. Res.,* **112,** D09108, doi:10.1029/2006JD008033.

——, W. T. Crow, and C. L. Keppenne, 2008: An adaptive ensemble Kalman filter for soil moisture data assimilation. *Water Resour. Res.,* **44,** W03423, doi:10.1029/2007WR006357.

——, M. G. Bosilovich, W. T. Crow, R. D. Koster, S. V. Kumar, S. P. P. Mahanama, and B. F. Zaitchik, 2009: Recent advances in land data assimilation at the NASA Global Modeling and Assimilation Office. *Data Assimilation for Atmospheric, Oceanic and Hydrologic Applications,* S. K. Park and L. Xu, Eds., Springer Verlag, 407–428.

Rienecker, M. M., and Coauthors, 2008: *The GEOS-5 Data Assimilation System—Documentation of Versions 5.0.1, 5.1.0, and 5.2.0*. Technical Report Series on Global Modeling and Data Assimilation, NASA/TM–2008–104606, Vol. 27, NASA, 118 pp. [Available online at http://gmao.gsfc.nasa.gov/pubs/docs/GEOS5_104606-Vol27.pdf.]

Rodell, M., and Coauthors, 2004: The Global Land Data Assimilation System. *Bull. Amer. Meteor. Soc.,* **85,** 381–394.